Steering polarization of infrared light through hybridization effect in a tri-rod structure

Jingxiao Cao,[1] Hui Liu,[1,3] Tao Li,[1] Shuming Wang,[1] Tianqi Li,[1] Shining Zhu,[1,4] and Xiang Zhang[2]

[1]*Department of Physics, National Laboratory of Solid State Microstructures, Nanjing University, Nanjing 210093, China*

[2]*5130 Etcheverry Hall, Nanoscale Science and Engineering Center, University of California, Berkeley, California 94720-1740, USA*

[3]*liuhui@nju.edu.cn*

[4]*zhusn@nju.edu.cn*

Received July 20, 2009; revised September 1, 2009; accepted September 3, 2009; posted September 10, 2009 (Doc. ID 114369); published October 13, 2009

A tri-rod structure (TRS), which can be seen as a combination of the double-rod structures reported by V. M. Shalaev *et al.* [Opt. Lett. **30**, 3356 (2005)10.1364/OL.30.003356], is proposed to control the polarization state of an electromagnetic (EM) wave in the near-infrared range. When a plane EM wave propagates through the TRS system, two orthogonal hybrid magnetic eigenmodes are established as a result of the strong hybridization effect. Thus, linearly polarized infrared light is shown to change its polarization around the resonance range after passing through an array of TRSs. The wavelength dependence of the polarization state is also calculated, and various polarized waves can be obtained. A metamaterial made of a large number of TRSs could be utilized as a polarization controllable medium with possible applications in optical elements and devices. © 2009 Optical Society of America

OCIS codes: 160.3918, 250.5403, 260.5430.

1. INTRODUCTION

In 1999, Pendry *et al.* proposed a nonmagnetic metallic element to achieve a strong resonant response to the magnetic component of the incident EM wave [1]. Since then, the magnetic resonance effect in metallic nanostructures has attracted considerable attention [2–15]. Coupling to the incident EM wave, these structures provide negative permeability. Combined with an electric response that has negative permittivity, such metallic nanostructures could achieve negative refraction [16–20], novel photon tunneling [21,22], and cloaking material [23] in the process.

On the other hand, polarization control in magnetic resonance structures has also been demonstrated [13,24–27]. Two coupled split-ring resonators [13,24] can be used to manipulate the polarization state by means of the hybridization effect of magnetic resonances. Manipulating optical rotation is realized in the extraordinary transmission through the L-shaped holes array in silver film by hybrid plasmonic excitations [25]. For the stacked-holes array metamaterial, polarization selection for the transmitted waves is obtained as a result of the negative index of refraction for one of its linearly polarized eigenwaves [26]. Moreover, wave polarizations in a model system consisting of an anisotropic homogeneous metamaterial layer were studied [27] recently. The polarization states of the reflected beam are altered because of the anisotropic property in the model. Because the magnetic response at optical range requires quite a small size (several hundred nanometers) and conventional magnetic resonators, such as split-ring resonators, are too complex to be fabricated at this size scale, some simpler designs are needed.

The nanorod pair proposed by Shalaev *et al.* is a quite simple structure for realizing magnetic resonance at optical frequencies [2]. Our previous paper proposed that a triple-rod (tri-rod) structure (TRS), which is seen as a combination of two double-rod structures (DRSs), could be used to realize omnidirectional negative refraction with broad bandwidth because of strong magnetic coupling in the structure [12]. It will be demonstrated in the current research that the TRS could also be used to manipulate polarization of the light. Results are expected to show that when a linear polarized infrared light passes through the metamaterial of the TRS, its polarization will change around the magnetic resonances. Various polarizations could be obtained continually corresponding to the different wavelength of the incident wave.

2. LAGRANGIAN FORMALISM AND HYBRIDIZATION MODEL

The unit cell of the general TRS is shown in Fig. 1(a), which includes three gold rods, A, B, and C, with circular cross sections. The TRS can be looked as two equivalent LC circuits, composed of magnetic loop (the metal rods) with inductance L and capacitor (the gaps between the rods) with capacitance C as represented in Fig. 1(b). A planar square array of the TRS is shown in Fig. 1(c). The lattice period is set at 500 nm, and the incident EM wave propagates in the y direction with the incident polarization angle θ shown in Fig. 1(c). The background is defined

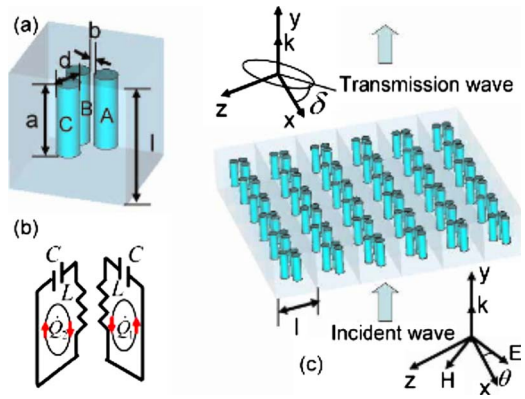

Fig. 1. (Color online) (a) Structure of a cubic unit cell of the TRS with $d=100$ nm, $a=300$ nm, $b=20$ nm, and $l=500$ nm. (b) Equivalent LC circuit of the TRS. (c) Metamaterial made of the TRS. The polarization and direction of the incident EM wave are represented.

as vacuum. If the host media is another dielectric material such as glass, the resonance frequencies can have a little redshift, but the physics is identical.

As the TRS can be seen as two coupled Shalaev DRSs, the resonance behavior of the TRS can be looked as the hybridization of the two DRSs. To explain the hybridization effect in the TRS better, the Lagrangian formalism is introduced [13]. Assume the total oscillatory charges Q_i accumulated in the gaps i ($i=1,2$) is defined as a generalized coordinate; the Lagrangian of the TRS can be expressed as

$$\mathfrak{J}_0 = (L/2)(\dot{Q}_1^2 + \dot{Q}_2^2) - (1/2C)(Q_1^2 + Q_2^2) + M\dot{Q}_1\dot{Q}_2. \quad (1)$$

The first term on the right-hand side of Eq. (1) is the kinetic energy of the oscillations. The second term is the electrostatic energy stored in the capacitive gaps A–B and B–C. The last term $M\dot{Q}_1\dot{Q}_2$ is related to the magnetic inductive energy between the two DRSs. By substituting $\mathfrak{J}_0$ in the Euler–Lagrange equation,

$$\frac{\mathrm{d}}{\mathrm{d}t}\left(\frac{\partial \mathfrak{J}_0}{\partial \dot{Q}_i}\right) - \frac{\partial \mathfrak{J}_0}{\partial Q_i} = 0 \quad (i=1,2), \quad (2)$$

it is straightforward to obtain two eigenwavelengths: $\lambda_\alpha = \lambda_0\sqrt{(1-\kappa)}$ and $\lambda_\beta = \lambda_0\sqrt{(1+\kappa)}$, where $\lambda_0 = 2\pi c\sqrt{LC}$ corresponds to the resonance wavelength of single DRS without any coupling interaction (c is the velocity of light in free space) and $\kappa = M/L$ is the magnetic coupling coefficient between the two pairs. Because of the coupling interaction between the two DRS resonators, the original resonance energy level λ_0 is split into two new hybrid resonance energy levels λ_α and λ_β. Because the magnetic response of the TRS is excited by the incident magnetic field, the induced currents oscillate in the opposite directions for the high-energy mode ($\dot{Q}_1 = -\dot{Q}_2$) but along the same direction for the low-energy mode ($\dot{Q}_1 = \dot{Q}_2$) in the shared rod B, shown in Figs. 2(d) and 2(f).

3. RESULTS AND DISCUSSION

To study the resonance mode characters of the proposed structure, a commercial software package CST MICRO-

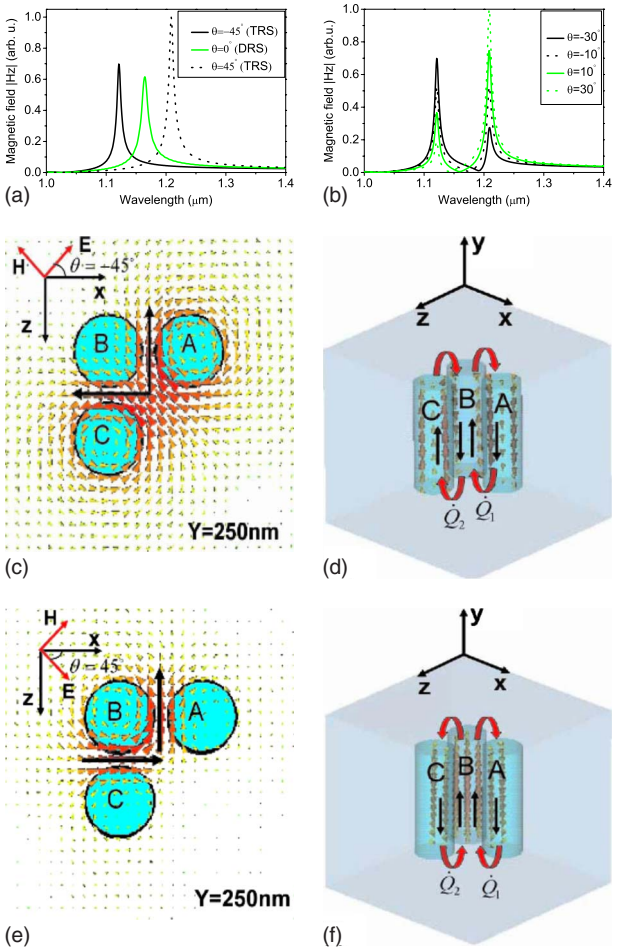

Fig. 2. (Color online) (a) Local magnetic field amplitude $|H_z|$ detected between rods A and B for the TRS (black solid curve for $\theta=-45°$ and black dotted curve for $\theta=45°$) and DRS [green (gray) solid curve for $\theta=0°$]. (b) Magnetic field amplitude $|H_z|$ calculated between rods A and B of the TRS for incident polarizations $\theta=-30°$, $-10°$, $10°$, $30°$. Local magnetic field vector profiles and current distributions (c)–(d) for the $|\alpha\rangle$ mode at $\lambda_\alpha=1.122$ μm with $\theta=-45°$ and (e)–(f) for $|\beta\rangle$ mode at $\lambda_\beta=1.211$ μm with $\theta=45°$.

WAVE STUDIO (Computer Simulation Technology GmbH, Darmstadt, Germany) was employed to obtain numerical analysis. In the calculations, the metal permittivity is satisfied with the Drude model: $\varepsilon(\omega)=1-\omega_p^2/(\omega^2+i\omega_\tau\omega)$, where ω_p is the bulk plasma frequency and ω_τ is the relaxation rate. For gold, the characteristic frequencies, which are fitted to the experimental data, are $\omega_p=1.37\times10^4$ THz and $\omega_\tau=40.84$ THz.

A monochromatic linear polarized wave $\mathbf{E}_i = E_0(\cos\theta\hat{x} + \sin\theta\hat{z})$ is used to excite the TRS. As is presented in Fig. 1(c), the plane wave propagates in the y direction (along the rod) with the incident polarization angle θ. In our simulations, a probe was placed at the center of the pair A–B to detect the local magnetic field. Figure 2 shows the recorded magnetic field H_z under different polarization angles. For comparison, the DRS system is also investigated, which includes only rods A and B. For the DRS, one resonance peak is obtained at $\lambda_0=1.172$ μm no matter how the polarization angle θ changes [the green (gray) curve in Fig. 2(a) with $\theta=0°$]. However, for the TRS, two

resonance peaks are observed in the curves: one is at $\lambda_\alpha = 1.122\ \mu$m with the incident polarization $\theta = -45°$ [the black solid curve in Fig. 2(a)] and the other is at $\lambda_\beta = 1.211\ \mu$m with the incident polarization $\theta = 45°$ [the black dotted curve in Fig. 2(a)]. For any other polarization case, both of the two resonance peaks can be obtained [the results for $\theta = -30°$, $-10°$, $10°$, $30°$ are given in Fig. 2(b)]. In order to investigate the specific nature of the resonance peaks of the TRS, local magnetic field and current distributions at these two resonance wavelengths are depicted in Figs. 2(c)–2(f). At $\lambda_\alpha = 1.122\ \mu$m, when the magnetic field vector in B–C is leftward, the magnetic field vector in A–B is upward [Fig. 2(c)]. The directions of the two currents induced in rod B are opposite [Fig. 2(d)]. At $\lambda_\beta = 1.211\ \mu$m, when the field vector in B–C is rightward, the field vector in A–B is upward [Fig. 2(e)]. The two currents induced in rod B have the same direction [Fig. 2(f)]. According to the Lagrangian theory above, we know these two resonance modes are $|\alpha\rangle$ and $|\beta\rangle$, respectively. Simultaneously, when $\theta = -45°$, only the mode $|\alpha\rangle$ can be excited; while $\theta = 45°$, only the mode $|\beta\rangle$ can be excited. For any other usual polarization angle, both $|\alpha\rangle$ and $|\beta\rangle$ modes are excited. Comparing the Lagrange results with the simulation, the magnetic coupling coefficient is retrieved as $\kappa \approx 0.068$.

Having determined the resonance properties of the proposed TRS, next we investigate the polarization change of the EM wave after it passes through the metamaterial composed of periodically arranged elements [see Fig. 1(c)]. In our simulations, the propagation direction of the EM wave is always kept in the y direction. But different polarization angles are used for the incident linearly polarized plane waves. The polarization change of the transmission wave is easily shown by observing the time evolution of the end of the point of the electric field vector when it travels through space. The trace of the end point is satisfied by the famous expression [28]

$$\left(\frac{E_x}{|E_x|}\right)^2 + \left(\frac{E_z}{|E_z|}\right)^2 - \frac{2E_xE_z}{|E_x||E_z|}\cos\phi = \sin^2\phi, \qquad (3)$$

where $|E_x|$ and $|E_z|$ are the amplitudes of the x and z electric components of the transmission wave. The phase difference ϕ between these two components is defined as $\phi = \phi_z - \phi_x$. When $\sin\phi = 0$, there is no phase difference between the x and z components and the transmission wave maintains a linear polarization state. When $\sin\phi < 0$, the electric vector rotates counterclockwise if an observer is facing the oncoming wave. The wave is left-hand polarized and has positive helicity. When $\sin\phi > 0$, the rotation of the electric vector is clockwise when looking into the wave. The wave is right-hand polarized and has a negative helicity.

In order to determine the polarization state of the transmission wave, the calculated transmission electric field curves under different polarization angles are given in Fig. 3 ($\theta = -45°$, $45°$, $-30°$, $30°$, $-10°$, $10°$). In the case $\theta = -45°$, $|E_x|$ and $|E_z|$ are equal [Fig. 3(a)], but the phase difference is $\phi = 180°$. In the case $\theta = 45°$, $|E_x|$ and $|E_z|$ still have the same value [Fig. 3(b)], but the phase difference is zero. Under the condition $\sin\phi = 0$, the transmission wave always maintains its linear polarization state for

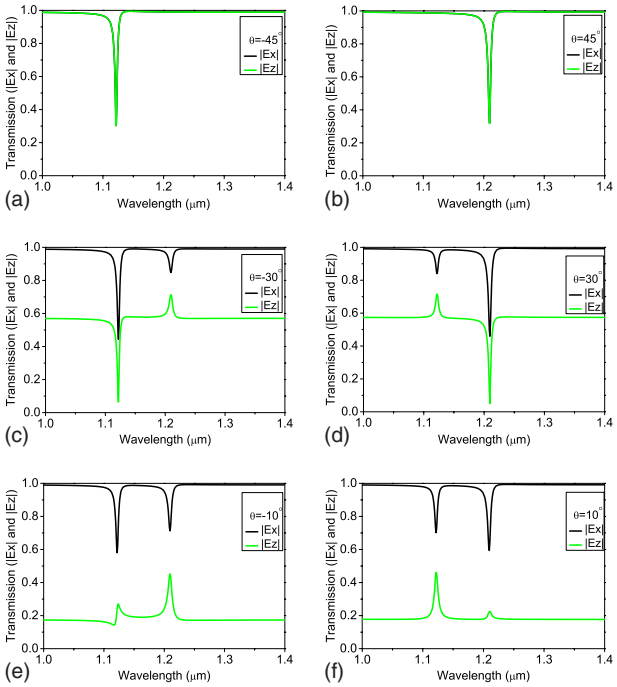

Fig. 3. (Color online) Amplitudes of the electric field components $|E_x|$ and $|E_z|$ when the plane wave passes through the metamaterial consisting of TRSs. The chosen incident polarization angles from (a) to (f) are $\theta = -45°$, $45°$, $-30°$, $30°$, $-10°$, $10°$.

these two incident polarization states. For other incident polarizations ($\theta = -30°$, $30°$, $-10°$, $10°$), the amplitudes $|E_x|$ and $|E_z|$ of the transmission wave are different around the resonance range as represented in Fig. 3(c)–3(f); the phase differences around the magnetic resonances are also shown in Fig. 4. It can be found that strong changes happen to the polarization state of the transmission wave. According to the sign of $\sin\phi$, the curves in Fig. 4 can be divided into three parts: when $\lambda_\alpha < \lambda < \lambda_\beta$, $\sin\phi$ is positive and the output wave presents the right-hand polarized state; when $\lambda < \lambda_\alpha$ or $\lambda > \lambda_\beta$, $\sin\phi$ is negative and the output wave shows the left-hand polarized state. In the calculations, $\theta = 0°$ is taken as an example to illustrate the general results. In Fig. 5, the polarization curves at six different wavelengths are given, which show that the polarizations are elliptic counterclockwise at about 1.110, 1.118, 1.213, and 1.220 μm, but the polarizations are elliptic clockwise at about 1.135 and 1.206 μm.

Generally, the principal axis of the curve followed by

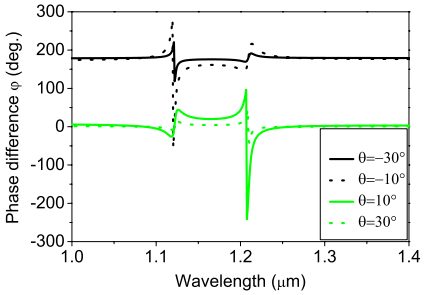

Fig. 4. (Color online) Phase difference between the two transmission electric components.

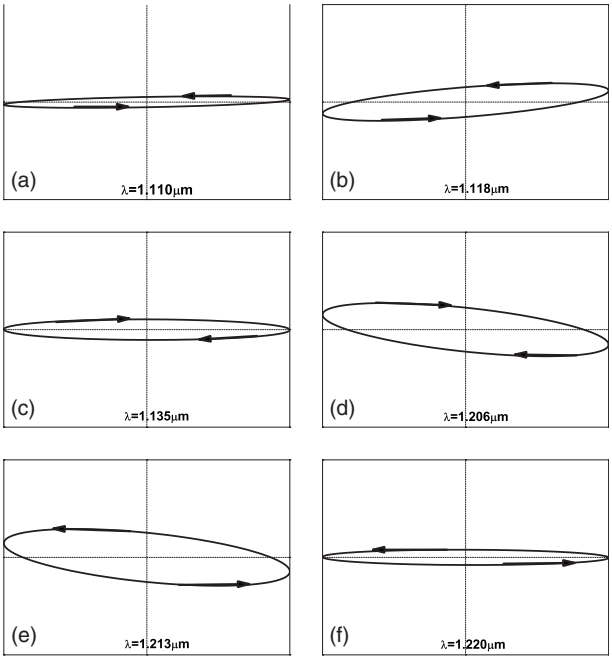

Fig. 5. Polarization patterns of the transmitted waves obtained at different wavelengths for the incident case $\theta=0°$. The arrows in the figures indicate the rotation directions of the transmission waves.

Eq. (3) is not along the x direction. The angle between them can be determined by the equation [28]

$$\tan(2\delta) = 2|E_x||E_z|\cos\phi/(|E_x|^2 - |E_z|^2). \tag{4}$$

The numerically calculated results for different incident polarizations ($\theta=-30°$, $30°$, $-10°$, $10°$) can be seen in Fig. 6. Notably, the rotation angle only changes around the magnetic resonance range in comparison with the incident polarization angle. By increasing the incident polarization angle $|\theta|$, the change in the rotation angle becomes weaker. When the incident polarization angle θ is $-45°$ or $45°$, the rotation angle does not change and keeps its original incident polarization, which is not shown in Fig. 6.

The mechanism behind the polarization change of the transmission wave can be understood after some physics analysis. Suppose the permittivity of the TRS is equal to ε_0, while the permeability of the TRS is a tensor. When excited by incident EM wave, the Lagrangian of the TRS can be written as

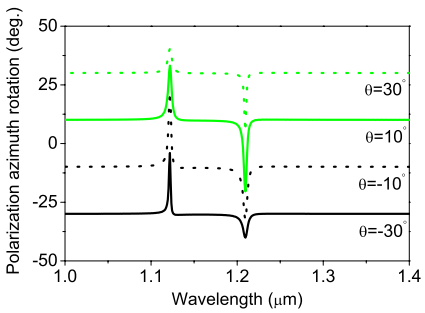

Fig. 6. (Color online) Rotation angle δ between the principal axis of the polarization for the transmitted wave and the x direction with different incident polarizations θ.

$$\Im_1 = (L/2)(\dot{Q}_1^2 + \dot{Q}_2^2) - (1/2C)(Q_1^2 + Q_2^2) + M\dot{Q}_1\dot{Q}_2 - m_x H_x^i - m_z H_z^i. \tag{5}$$

The induced moments $m_{x(z)}=s\dot{Q}_{2(1)}$ are related to the excitation field through $\mathbf{m}=\vec{\beta}\cdot\mathbf{H_i}$. The coefficient s is the effective area of the pair, and $\vec{\beta}$ is the magnetic polarizability tensor. Introducing Ohmic dissipation $\Re=(\sigma/2)(\dot{Q}_1^2+\dot{Q}_2^2)$, the damped Euler–Lagrangian equations can be written as [10]

$$\frac{\mathrm{d}}{\mathrm{d}t}\left(\frac{\partial\Im_1}{\partial\dot{Q}_i}\right) - \frac{\partial\Im_1}{\partial Q_i} = -\frac{\partial\Re}{\partial\dot{Q}_i} \quad (i=1,2). \tag{6}$$

Based on the damped Euler–Lagrangian equations, we obtain the induced currents, expressed as

$$\dot{Q}_1 = \frac{\kappa\omega^2 s' H_x - (\omega^2 + i\Gamma\omega - \omega_0^2)s' H_z}{(1-\kappa^2)(\omega^2 + i\gamma_\alpha\omega - \omega_\alpha^2)(\omega^2 + i\gamma_\beta\omega - \omega_\beta^2)},$$

$$\dot{Q}_2 = \frac{-(\omega^2 + i\Gamma\omega - \omega_0^2)s' H_x + \kappa\omega^2 s' H_z}{(1-\kappa^2)(\omega^2 + i\gamma_\alpha\omega - \omega_\alpha^2)(\omega^2 + i\gamma_\beta\omega - \omega_\beta^2)}, \tag{7}$$

where $s'=s/L$ is related to the effective area of the pair, ω_α and ω_β are the frequencies corresponding to λ_α and λ_β, and $\Gamma=\sigma/L$, $\gamma_{\alpha(\beta)}=\Gamma/(1\mp\kappa)$ are related to the lossiness for the two modes. According to the relationship between the induced magnetic moments $m_{x(z)}=s\dot{Q}_{2(1)}$ and the excitation field through $\mathbf{m}=\vec{\beta}\cdot\mathbf{H_i}$, the elements of the effective permeability tensor can be written as

$$\mu_{xx(zz)} = 1 - \frac{(\omega^2 + i\Gamma\omega - \omega_0^2)ss'}{(1-\kappa^2)(\omega^2 + i\gamma_\alpha\omega - \omega_\alpha^2)(\omega^2 + i\gamma_\beta\omega - \omega_\beta^2)},$$

$$\mu_{xz(zx)} = \frac{\kappa\omega^2 ss'}{(1-\kappa^2)(\omega^2 + i\gamma_\alpha\omega - \omega_\alpha^2)(\omega^2 + i\gamma_\beta\omega - \omega_\beta^2)}. \tag{8}$$

From Maxwell equations [29], we obtain two eigen-wavevectors in the TRS metamaterial as

$$k_\alpha = k_0\sqrt{\varepsilon_0\left(1 - \frac{ss'}{(1-\kappa)(\omega^2 + i\gamma_\alpha\omega - \omega_\alpha^2)}\right)},$$

$$k_\beta = k_0\sqrt{\varepsilon_0\left(1 - \frac{ss'}{(1+\kappa)(\omega^2 + i\gamma_\beta\omega - \omega_\beta^2)}\right)}, \tag{9}$$

where $k_0=\omega/c$ is the wave vector of the light in free space. Thus, the elements of the diagonal permeability tensor of the TRS metamaterial in the α–β coordinate system (the principal coordinate system) are expressed as

$$\mu_\alpha = 1 - \frac{ss'}{(1-\kappa)(\omega^2 + i\gamma_\alpha\omega - \omega_\alpha^2)},$$

$$\mu_\beta = 1 - \frac{ss'}{(1+\kappa)(\omega^2 + i\gamma_\beta\omega - \omega_\beta^2)}. \tag{10}$$

The corresponding polarization states of these two eigenwaves are

$$\hat{e}_\alpha = \frac{1}{\sqrt{2}}\begin{pmatrix} -\hat{x} \\ \hat{z} \end{pmatrix}, \quad \hat{e}_\beta = \frac{1}{\sqrt{2}}\begin{pmatrix} \hat{x} \\ \hat{z} \end{pmatrix}, \tag{11}$$

one of which represents the incident polarization state $\theta = -45°$, and the other is the state $\theta = 45°$ in the x–z coordinate system. Thus, the α–β coordinate system has the 45° rotation angle in the counterclockwise direction in respect to the x–z coordinate system. These agree well with the above simulation results. According to the theoretical model [16] and coordinate transformation theory, we attain the relationship between the incident and transmitted waves in the x–z coordinate system as follows:

$$\begin{pmatrix} E_x^t \\ E_z^t \end{pmatrix} = \frac{1}{2}\begin{pmatrix} (E_x^i - E_z^i)T_\alpha + (E_x^i + E_z^i)T_\beta \\ -(E_x^i - E_z^i)T_\alpha + (E_x^i + E_z^i)T_\beta \end{pmatrix}, \tag{12}$$

where the transmission coefficients of the TRS metamaterial along the principal axis directions are expressed as

$$T_{\alpha(\beta)} = \frac{4n_{\alpha(\beta)} \exp(-in_{\alpha(\beta)}k_0 d)}{(n_{\alpha(\beta)} + 1)^2 - (n_{\alpha(\beta)} - 1)^2 \exp(-2in_{\alpha(\beta)}k_0 d)}. \tag{13}$$

Here $n_{\alpha(\beta)} = \sqrt{\varepsilon_0 \mu_{\alpha(\beta)}}$ represents the corresponding indices of the two eigenstates. From Eq. (12), we can easily see that the transmitted wave changes its polarization around the resonance range because of the magnetic resonance coupling in the TRS metamaterial. Simultaneously, there is no polarization change for the eigenstates. According to the coordinate transformation method, we use the simulation transmission of the incident cases $\theta = \pm 45°$ to obtain the retrieved transmission amplitude results for the incident polarization cases $\theta = -30°$, 30°, −10°, 10° shown in Fig. 7, which agree well with the simulations represented in Fig. 3. If rods A and B are included per unit cell, the structure is symmetric. Thus the magnetic plasmon mode is induced by the incident magnetic field component H_z. The permeability of the system is a scalar ($\mu_x = 0$, $\mu_z \neq 0$). That is to say, the transmission wave includes only the EM wave components E_x and H_z.

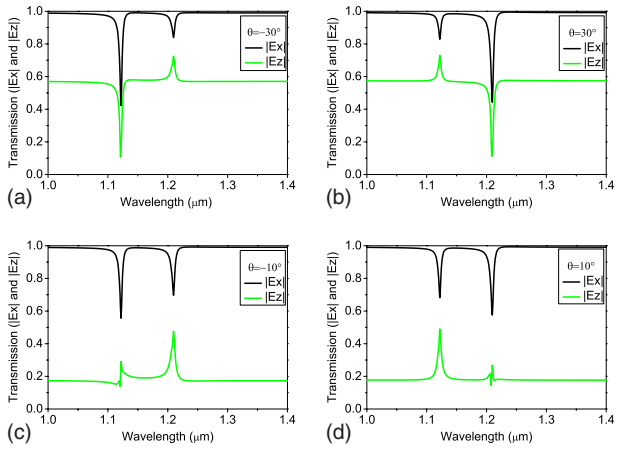

Fig. 7. (Color online) Retrieved amplitudes of the electric field components $|E_x|$ and $|E_z|$ by coordinate transformation theory. The chosen incident polarization angles from (a) to (d) are $\theta = -30°$, 30°, −10°, 10°.

4. CONCLUSION

The polarization properties of the transmission wave through a metamaterial composed of TRSs is thoroughly investigated. When a linearly polarized EM wave strikes the metamaterial, magnetic plasmon hybridization occurs and two magnetic plasmon eigenmodes are excited. Magnetic resonance coupling established in the TRS results in the polarization change of the transmitted wave. Various polarizations could be obtained through changing the incident wavelength. Optical elements, such as tunable polarizers and switches, are possible applications of the TRS-based complex media.

ACKNOWLEDGMENTS

This work was supported by the State Key Program for Basic Research of China (grants 2009CB930501, 2006CB921804, and 2004CB619003) and by the National Nature Science Foundation of China (NSFC) (grants 10604029, 10704036, 10874081, 10534042, and 60578034).

1. J. B. Pendry, A. Holden, D. Robbins, and W. Stewart, "Magnetism from conductors and enhanced nonlinear phenomena," IEEE Trans. Microwave Theory Tech. **47**, 2075–2084 (1999).
2. V. M. Shalaev, W. S. Cai, U. K. Chettiar, H. K. Yuan, A. K. Sarychev, V. P. Drachev, and A. V. Kildishev, "Negative index of refraction in optical metamaterials," Opt. Lett. **30**, 3356–3358 (2005).
3. T. J. Yen, W. J. Padilla, N. Fang, D. C. Vier, D. R. Smith, J. B. Pendry, D. N. Basov, and X. Zhang, "Terahertz magnetic response from artificial materials," Science **303**, 1494–1496 (2004).
4. S. Linden, C. Enkrich, M. Wegener, J. F. Zhou, T. Koschny, and C. M. Soukoulis, "Magnetic response of metamaterials at 100 terahertz," Science **306**, 1351–1353 (2004).
5. N. Katsarakis, G. Konstantinidis, A. Kostopoulos, R. S. Penciu, T. F. Gundogdu, M. Kafesaki, E. N. Economou, Th. Koschny, and C. M. Soukoulis, "Magnetic response of split-ring resonators in the far-infrared frequency regime," Opt. Lett. **30**, 1348–1350 (2005).
6. C. Enkich, M. Wegener, S. Linden, S. Burger, L. Zschiedrich, F. Schmidt, J. F. Zhou, Th. Koschny, and C. M. Soukoulis, "Magnetic metamaterials at telecommunication and visible frequencies," Phys. Rev. Lett. **95**, 203901 (2005).
7. J. Zhou, Th. Koschny, M. Kafesaki, E. N. Economou, J. B. Pendry, and C. M. Soukoulis, "Saturation of the magnetic response of split-ring resonators at optical frequencies," Phys. Rev. Lett. **95**, 223902 (2005).
8. A. Ishikawa, T. Tanaka, and S. Kawata, "Negative magnetic permeability in the visible light region," Phys. Rev. Lett. **95**, 237401 (2005).
9. A. N. Grigorenko, A. K. Geim, H. F. Gleeson, Y. Zhang, A. A. Firsov, I. Y. Khrushchev, and J. Petrovic, "Nanofabricated media with negative permeability at visible frequencies," Nature **438**, 17–20 (2005).
10. H. Liu, D. A. Genov, D. M. Wu, Y. M. Liu, J. M. Steele, C. Sun, S. N. Zhu, and X. Zhang, "Magnetic plasmon propagation along a chain of connected subwavelength resonators at infrared frequencies," Phys. Rev. Lett. **97**, 243902 (2006).
11. T. Li, H. Liu, F. M. Wang, Z. G. Dong, S. N. Zhu, and X. Zhang, "Coupling effect of magnetic polariton in perforated metal/dielectric layered metamaterials and its influence on negative refraction transmission," Opt. Express **14**, 11155–11163 (2006).
12. F. M. Wang, H. Liu, T. Li, S. N. Zhu, and X. Zhang, "Omnidirectional negative refraction with wide bandwidth introduced by magnetic coupling in a tri-rod structure," Phys. Rev. B **76**, 075110 (2007).
13. H. Liu, D. A. Genov, D. M. Wu, Y. M. Liu, C. Sun, S. N. Zhu,

and X. Zhang, "Magnetic plasmon hybridization and optical activity at optical frequencies in metallic nanostructures," Phys. Rev. B **76**, 073101 (2007).
14. Na Liu, Hui Liu, Shining Zhu, and Harald Giessen, "Stereometamaterials," Nature Photon. **3**, 157–162 (2009).
15. A. Alu, A. Salandrino, and N. Engheta, "Negative effective permeability and left-handed materials at optical frequencies," Opt. Express **14**, 1557–1567 (2006).
16. J. B. Pendry, "Negative refraction makes a perfect lens," Phys. Rev. Lett. **85**, 3966–3969 (2000).
17. D. R. Smith, J. B. Pendry, and M. C. K. Wiltshire, "Metamaterials and negative refractive index," Science **305**, 788–792 (2004).
18. S. Linden, C. Enkrich, G. Dolling, M. W. Klein, J. F. Zhou, T. Koschny, C. M. Soukoulis, S. Burger, F. Schmidt, and M. Wegener, "Photonic metamaterials: magnetism at optical frequencies," IEEE J. Sel. Top. Quantum Electron. **12**, 1097–1105 (2006).
19. C. M. Soukoulis, S. Linden, and M. Wegener, "Negative refractive index at optical wavelengths," Science **315**, 47–49 (2007).
20. N. Fang, H. Lee, C. Sun, and X. Zhang, "Sub-diffraction-limited optical imaging with a silver superlens," Science **308**, 534–537 (2005).
21. Z. M. Zhang and C. J. Fu, "Unusual photon tunneling in the presence of a layer with a negative refractive index," Appl. Phys. Lett. **80**, 1097 (2002).
22. K.-Y. Kim, "Photon tunneling in composite layers of negative- and positive-index media," Phys. Rev. E **70**, 047603 (2004).
23. D. Schurig, J. J. Mock, B. J. Justice, S. A. Cummer, J. B. Pendry, A. F. Star, and D. R. Smith, "Metamaterial electromagnetic cloak at microwave frequencies," Science **314**, 977–980 (2006).
24. T. Q. Li, H. Liu, T. Li, S. M. Wang, F. M. Wang, R. X. Wu, P. Chen, S. N. Zhu, and X. Zhang, "Magnetic resonance hybridization and optical activity of microwaves in a chiral metamaterial," Appl. Phys. Lett. **92**, 131111 (2008).
25. T. Li, H. Liu, S. M. Wang, X. G. Yin, F. M. Wang, S. N. Zhu, and X. Zhang, "Manipulating optical rotation in extraordinary transmission by hybrid plasmonic excitations," Appl. Phys. Lett. **93**, 021110 (2008).
26. M. Berute, M. Navarro-Cia, M. Sorolla, and I. Campillo, "Polarization selection with stacked hole array metamaterial," J. Appl. Phys. **103**, 053102 (2008).
27. J. Hao, Yuan Yu, L. Ran, Jiang Tao, J. A. Kong, C. T. Chan, and L. Zhou, "Manipulating electromagnetic wave polarizations by anisotropic metamaterials," Phys. Rev. Lett. **99**, 063908 (2007).
28. J. D. Jackson, *Classical Electrodynamics* (Wiley, 1999).
29. A. Yariv and P. Yeh, *Optical Waves in Crystals: Propagation and Control of Laser Radiation* (Wiley, 1984).